J Nanopart Res (2021) 23: 97
https://doi.org/10.1007/s11051-021-05194-5

RESEARCH PAPER

Titania containing natural clay doped with carbon nanotubes for enhanced natural photocatalytic discoloration of wastewater

A. A. Muleja · M. P. Mubiayi · F. Hassard · B. B. Mamba

Received: 18 June 2020 / Accepted: 22 March 2021 / Published online: 17 April 2021

Abstract Water contamination with dyes is harmful to humans and the environment. This study investigated the photocatalytic activity of natural clay (GOL) mixed with carbon nanotubes (CNT) for removal of brilliant black (BB) in wastewater. The materials were characterized with FESEM-EDS, XRD, XRF, FTIR and UV-vis DRS. The natural clay contains 2.34 % TiO_2 which is 75% more than most natural clays. SEM showed that CNT were well dispersed and mixed with clay. DRS spectra showed two absorption bands above 380 nm. CNT in GOL has decreased significantly the energy band gaps from 2.75 and 3.25 eV to 1.53 and 2.90 eV for GOL and 10% CNT–GOL, respectively. Photocatalytic activity was enhanced with degradation of BB increased from 66 to 95% with GOL and 10% CNT–GOL respectively after 45 min of visible light irradiation. The improvement can be attributed to the synergy of the interface heterojunction of clay and CNT. The presence of CNT reduces the e^- and h^+ (e^- / h^+) pairs recombination and facilitates the production of reactive oxygen species responsible for the decay of dye. The addition of H_2O_2 to the experiment (2 mmoL) confirmed the role of holes and hydroxyl radicals. Eighty-five percent of BB carbon content was removed with 10% CNT–GOL suggesting that mineralization occurred. After 45 min of visible light irradiation, the degradation kinetic studies followed a second-order reaction with a $R^2 = 0.997$. Therefore, natural clay–CNT nanocomposites can be applied to treat dyes containing wastewaters.

Keywords African clay · Nanocomposites · Mechanical mixing · Heterojunction · Photocatalysis · Dyes

This article is part of the topical collection: Nanotechnology Convergence in Africa

Guest Editors: Mamadou Diallo, Abdessattar Abdelkefi, and Bhekie Mamba

A. A. Muleja (✉) · M. P. Mubiayi · F. Hassard · B. B. Mamba (✉)
Institute for Nanotechnology and Water Sustainability (iNanoWS), College of Science, Engineering and Technology, University of South Africa, Florida Campus, Johannesburg 1710, South Africa
e-mail: mulejaa@unisa.ac.zae-mail: mambabb@unisa.ac.za

M. P. Mubiayi
Mechanical and Industrial Engineering Department, College of Science, Engineering and Technology, University of South Africa, Florida Campus, Johannesburg 1710, South Africa

F. Hassard
Cranfield University, College Way, Bedford, Bedfordshire MK43 0AL, UK

Introduction

The exploitation of industrial dyestuffs generates significant amounts of organics contamination in water through release of contaminated effluents. Azo compounds such as brilliant black (BB) are a complex class of dyes having a wide range of applications in textile, food, paint, plastics and cosmetics industries. The release of azo dyes into the environment is of great concern due to the colouration of natural waters, their

toxicity and the possibility of mutagenic and carcinogenic breakdown products (Oh et al. 1997; Rafii et al. 1997; Li and Bishop 2002; Todorova et al. 2014; Brüschweiler and Merlot 2017; Kausar et al. 2018). Traditional methods for the disposal of dyes in wastewaters (e.g. filtration, coagulation, ion-exchange, granular activated carbon and ion exchange resins) are costly and generate hazardous secondary pollution problems (Molinari et al. 2017). Traditional advanced oxidation processes (AOPs) offer enhanced dye destruction and low by-product and secondary pollution problems compared to traditional dye treatments (Al-Kdasi et al. 2004). Natural methods for dye decolourization such as clays adsorbents have gained attention as they are inexpensive, can be sourced local to pollution source and empower community led treatment initiatives (Kausar et al. 2018). However, dye treatment using natural clays can result in secondary pollution through desorption into water courses. Thus, there is a need for the development of new technologies that can remove these hazardous compounds in water and wastewater (Al-Kdasi et al. 2004; Molinari et al. 2017). Therefore, the synergy of adsorption, degradation and mineralization of the dyes by enhanced materials represents a strategy to treat dyes at source.

Photocatalytic oxidation of organic compounds present in wastewater using photochemical reaction occurring on a semiconductor catalytic solid surface activated by solar light irradiation has shown promise for dye treatment (Saleh and Gupta 2012). Chen et al. (2004) found that adsorption is significantly effective to enhance the rate of photodegradation of dyes under visible light irradiation. Herrmann (1999) reported that photocatalysis relies on the aptitude of the photocatalyst to simultaneously adsorb both reactants and to absorb efficient photons and the migration of light-induced electron holes. Titania (TiO_2) is an effective photocatalyst as it has a large band gap energy, physico-chemical stability, non-toxic, cost-effectiveness and is insoluble. However, the efficiency of TiO_2 is reduced due to e^- / h^+ pair recombination. Adding a co-adsorbent is a good strategy for increasing the photocatalytic efficiency of TiO_2 (Saleh and Gupta 2012). It is therefore expected that using natural clays would combine the advantages (adsorption and photoresponse) of each compound of the reported materials (Asif et al. 2015; Hamza et al. 2018; Martínez-Costa et al. 2018) to enhance the removal of dyes pollutants from dye-containing wastewaters. Natural clays could be utilized as photocatalysts due to the high photochemical activity in the degradation of contaminants, high chemical stability, accessibility and low cost (Martínez-Costa et al. 2018). For instance, da Silva Lopes et al. (2019) have recently indicated that the mixture of the TiO_2 dispersion with purified natural kaolinite resulted in the formation of nanocomposites with good catalytic properties.

CNT can be produced in a semi-conducting, semimetallic or metallic form (Ebbesen et al. 1996; Collins and Avouris 2000). We hypothesised that CNT could significantly enhance GOL photocatalytic performance as CNT acts as a semiconductor reducing e^- / h^+ pairs recombination. CNT is thought to improve photocatalysis of complex organic molecules through positive h^+ formation in the valence band, and e^- occupied the conduction band which generates radicals. If the e^- / h^+ pairs recombine, the photocatalytic efficiency is reduced. The combination of CNT with other materials leads to a new generation of donor-acceptor nanocomposites, which, upon illumination, give a fast charge separation and a slow charge recombination. CNT should be even more suitable for achieving charge transfer and charge transport (Guldi et al. 2005). Indeed, some studies (Saleh and Gupta 2012; Yin et al. 2016) have proven that the e^- accepting and e^- transport properties of CNT provide a convenient way to direct the flow of photogenerated charge carriers. The excited e^- in the conduction band of TiO_2 may migrate into CNT, of which have a special structure and the ability for e^- transport. Thus, the possibility of the recombination of e^- / h^+ pairs decreases more radicals in the system, resulting in faster degradation of the dyes (Yu et al. 2005). Natural clays rarely contain sufficient TiO_2 considered > 1 wt% for enhanced photocatalysis (Hamza et al. 2018; Martínez-Costa et al. 2018). In this study, natural clay from Golf–Katanga region (GOL clay) in the DR Congo was used due to a TiO_2 content > 1 %. The method to mechanically mix different materials such as zeolite and TiO_2 (Yamaguchi et al. 2009) and TiO_2 with MgAl-LDH (Paredes et al. 2011) to form composites with high performance photocatalytic properties has been reported previously. To the best of our knowledge, GOL and CNT have not been used previously for the removal of dyes from water. Therefore, the aim of this study is to (i) understand the impact of CNT dose (5 and 10 wt%) on the photocatalytic performance and (ii) investigate whether the azo dye compound could be mineralized using natural solar radiation. The photocatalytic activity was achieved through controlled degradation experiments using these materials under visible light irradiation. The

superior adsorption ability of the photocatalytic materials (GOL mixed CNT) was used to the advantage of photodegradation to ensure enhanced capture, degradation and mineralization of dyes molecules (Yu et al. 2005; Asif et al. 2015; Hamza et al. 2018; Martínez-Costa et al. 2018). The principal focus of this investigation was solely on the photocatalytic activity of the mixed nanocomposites.

Experimental methods

Materials

The natural clays used in this study originated from Golf coded as GOL, Katanga province in the Democratic Republic of the Congo (DRC). Multi-walled carbon nanotubes (CNT) were produced from ferrocene (2.0 g) dissolved in toluene (50.0 mL) through a nebulized spray pyrolysis (NSP) technique reported in the literature (Muleja et al. 2012). A modified method to mechanically mix two materials into photocatalysts was followed (Yamaguchi et al. 2009). Briefly, the GOL clay was pulverized using a Siebtechnik Puck Mill Ring Mill Pulverizer and mechanically mixed with CNT to make 3 different ratios. The ratios represented are 100/0 (% w/w) for 100% GOL–0 % CNT; 95/5 (% w/w) for 95% GOL–5 % CNT and 90/10 (% w/w) for 90% GOL–10 % CNT. The mixture was then thoroughly ground resulting in homogeneous products. The brilliant black (BB: dye content 60 %) and the hydrogen peroxide solution (H_2O_2: > 30 %) were purchased from Sigma-Aldrich. Milli-Q ultrapure water was used throughout the experiments unless otherwise stated.

Characterization of GOL, 5% CNT–GOL and 10% CNT–GOL

The X-ray fluorescence (XRF) analysis using a Rigaku, ZSX Primus II was performed on the GOL sample to obtain the chemical composition. Pallets of GOL sample were made and dry in an oven for 24 h to remove the moisture. Bulk chemical compositions (phase identification) of the GOL and the admixtures were recorded on a XRD (Ultima IV X-ray diffractometer, Rigaku) equipped with a graphite-monochromated Cu Kα radiation source (40 kV, 30 mA) with 2θ range of 10 to 90°, step size of 0.01 and scan speed of 0.5° min^{-1}. A JEOL JSM-7800F Field Emission Scanning Electron Microscope (FESEM) instrument coupled with Thermo Scientific Ultradry energy-dispersive X-ray spectroscopy (EDS) detector was used for the surface morphology analysis and to identify chemical elements and their distribution on the samples. The Fourier transform infrared spectroscopy (FTIR) spectra of the samples were recorded by using a Perkin–Elmer Frontier FTIR spectrometer. The samples were scanned with 16 background accumulations in the range of 450–4000 cm^{-1} at the spectral resolution of 4 cm^{-1} by using the KBr pellet method. A PerkinElmer LAMBDA 1050 UV/VIS/NIR spectrometer was combined with a reference material comprised of barium sulphate. The diffuse reflection spectroscopy (DRS) was acquired in the range of 200 to 800 nm. Absorption spectra were transformed according to the Kubelka−Munk relationship to understand the absorption characteristics of our materials and calculate the optical band gaps. The total organic content (TOC) measurements were carried out using a TOC torch (Teledyne Tekmar, USA) instrument. Standard solutions of 0 ppm, 5 ppm, 10 ppm, 25 ppm and 50 ppm carbon were prepared using potassium hydrogen phthalate (KHP) and DI water. Calibration standards were measured prior to sample analysis for instrument calibration.

Photocatalytic degradation evaluation

The photocatalytic degradation experiments were carried in a similar manner as previously reported (Muleja and Mamba 2018). In brief, degradation experiments were undertaken in a solar simulator (HAL–320 Asahi Spectra, Japan) which produced the required spectral irradiance and dose. A 300 W Compact Xenon light with apparent power 500 VA was used as the light source. The solar simulator radiation spectrum output wavelength ranges were set from 350 to 1100 nm, and an air mass filter (1.5 global filter) was placed in front of the lamp to eliminate most of the UV radiation. The intensity distance which was the distance from the collimator lens to the sample surface was set at 37 mm. It created an effective radiated area of 50 mm^2 and an irradiance of approximately 100 mW cm^{-2}. Typically, all the materials (25 mg) were mixed with BB solution (5ppm, 50 mL). The mixture was stirred in the dark for 60 min to establish the adsorption-desorption equilibrium. A sample was drawn from the solution using a syringe unit fitted with 0.45-μm pore size hydrophilic PVDF membrane. The first sample drawn after

adsorption-desorption equilibrium was considered as the initial concentration (C_i). The solar simulator was prewarmed (30 min) for stable irradiance output, and samples (mixed solution of photocatalysts and BB) were subsequently irradiated in a 100-mL quartz beaker. Samples were drawn from the solution at 15-min intervals, filtered and analysed using a UV-vis spectrometer (Lambda 650S, Perkin Elmer, USA). The experiments were undertaken for 60 min and were stirred using a magnetic bar. The UV-vis photometric measurements of standards and samples were done at maximum absorbance 571.3 nm (BB wavelength: 567–573 nm) to obtain the concentration of BB after the elapsed time interval (C_f). Experimental data from the effect hydrogen peroxide solution on the photocatalytic degradation of BB were collected in the similar manner, except that H_2O_2 was added to the mixed solution (BB and all three materials) and at various concentrations, namely, 2 mmoL, 4 mmoL and 6 mmoL. A calibration curve was obtained from the standards, and the percentage photocatalytic removal of BB dye was calculated after Eq. (1):

$$\%\text{Degradation} = \frac{C_i - C_f}{C_f} \times 100 \quad (1)$$

Results and discussion

Morphology analysis of CNT, GOL and 10 % CNT–GOL

The micrographs of three materials namely the CNT, GOL and 10% CNT–GOL are shown in Fig. 1 (a–d). CNT morphology (Fig. 1 (a)) were significantly different compared to the clay (Fig. 1 (b)). However, when the two were mixed, the surface morphology of these materials shows the presence of well-dispersed clay consisting of particles of different sizes forming blocks of variable thickness in Fig. 1 (c) at the micrometre resolution. When the resolution was lowered in the nanometre, nanotubes are clearly visible on the nanocomposite 10 % CNT–GOL as shown in Fig. 1 (d). High magnification image of FESEM depicted in Fig. 1 (b) showed layers on the natural clay (raw GOL). The presence of these layers could be crucial for the removal of BB dyes, through provision of effective photocatalytic reaction area. The raw GOL sample also showed pore structures which represent an advantage for adsorption and subsequently photocatalytic activity (Fig. 1 (b)). The high-definition SEM pictures of the mixed materials (Fig. 1 (c) and (d)) are composed of carbon nanotubes well mixed with clays cumulative form of aggregated different-shaped particles. The incorporation of CNT appeared on the surface of clay as previously reported (Gournis et al. 2002; Terzopoulou et al. 2016).

Characterization of 10 % CNT–GOL elemental composition

Elemental mapping analysis of GOL clay and GOL clay mixed with CNT was measured. The elemental distribution of 10% CNT–GOL clay show the presence of elements such as oxygen (O), silicon (Si), aluminium (Al), iron (Fe), potassium (K) and titanium (Ti) (Fig. 2a) which is expected and in agreement with previous reports on natural clays (Yu et al. 2005; Martínez-Costa et al. 2018). The energy-dispersive X-ray spectroscopy (EDS) spectrum of 10% CNT–GOL clay sample confirming the presence of each element is found by the mapping analysis (Fig. 2b). The elemental distribution on the maps indicates that the intensity of elements O, Si, Al, Fe, K and Ti follow a decreasing order, respectively. The results reveal a high concentration of Si and Al while Fe, K and Ti are less abundant. Further analysis of the surface topography showed that GOL are dominated by oxygen and the following mineral phases including SiO_2, Al_2O_3, TiO_2 and Fe_2O_3 which offer varying levels of photocatalytic activity (Martínez-Costa et al. 2018).

Chemical composition determination of GOL clay

CNT–GOL clay sample was not analysed because X-ray fluorescence (XRF) is limited to detect carbon content. The chemical composition of GOL clay was determined with XRF spectrometer (Table 1) and has a similar profile to other natural clays (Martínez-Costa et al. 2018). However, the concentration of TiO_2 is higher (2.34%) than for the other natural clays, 0 % (Hamza et al. 2018) and 0.58 % (Martínez-Costa et al. 2018), which is an advantage of the GOL clay because TiO_2 is often desired for photocatalytic activity. The high contents of silica, alumina, hematite and titania are of great importance for the application of these materials in photocatalysis. Additionally, the clay and its composition, namely, silica, alumina, hematite and

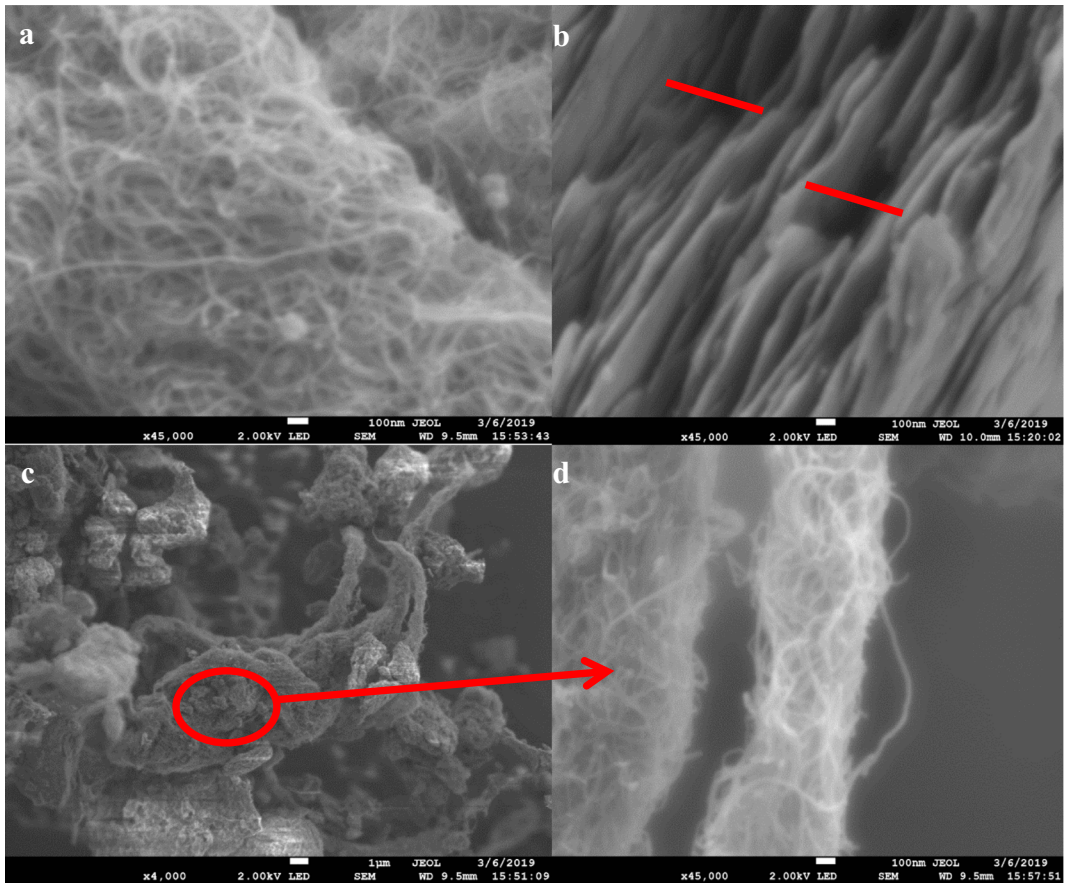

Fig. 1 FESEM surface morphology images of (a) CNT, (b) GOL clay, (c) low magnification 10% CNT–GOL and (d) high magnification of 10% CNT–GOL. Red lines represent pores and layers

titania have been used significantly in the adoption of contaminants from aqueous solution separately and or combined with other compounds (Kausar et al. 2018). Moreover, Hermann (1999) has reported that adsorption is a crucial stage of the photocatalysis process. The XRF results shown in Table 1 display the presence of chemical elements, namely, O, Si, Al, Fe, K and Ti which is consistent with the EDS analysis in Fig. 2.

Chemical phases determination and functional groups identification of GOL, 5% CNT–GOL and 10 % CNT–GOL

The X-ray diffraction (XRD) patterns of GOL clay (black colour), 5% CNT–GOL clay (red colour) and 10% CNT–GOL clay (green colour) samples are shown in Fig. 3a. The XRD technique was instrumental to determine the bulk structure and composition of materials with crystalline structure. The analysis revealed that GOL are constituted by mineral phases including quartz (SiO_2) (ICDD (PDF2010): 01-082-1572), cristobalite (SiO_2), karrooite ($MgTi_2O_5$) (ICDD (PDF2010): 01-075-9297), perovskite ($Ca(TiO_3)$ (ICDD (PDF2010): 01-088-0790) and mullite ($Al_5SiO_{9.5}$) (ICDD (PDF2010): 01-088-2049). The presence of silicon is evidence of SiO_2 as shown at peaks 2-theta ranging from 21° cristobalite (1,1,3), silicon dioxide (1,1,1) and cristobalite (1,0,1) to 28° silicon dioxide (3,0,0), karrooite (6,3,0), mullite (16,2,2) and perovskite (2,3,1). The shift in peaks was attributed to different phases of SiO_2 and probably the blending with CNT as well. Similar peaks at 2 θ = 26.8 ° are mullite, (11,1,3) and karrooite, (1,1,1) and 42.6° corresponding to graphite in a clay-multi-walled CNT sample have been reported previously (Zhu et al. 2004; Oh et al. 2010). The peaks corresponding to TiO_2 from karrooite (1,1,1), perovskite (1,3,1), mullite (10,2,0) and perovskite (1,2,0) are identified at 2 θ = 36.81, 45.77, 55.14 and 62.41, 77.90°, while quartz can also be found at

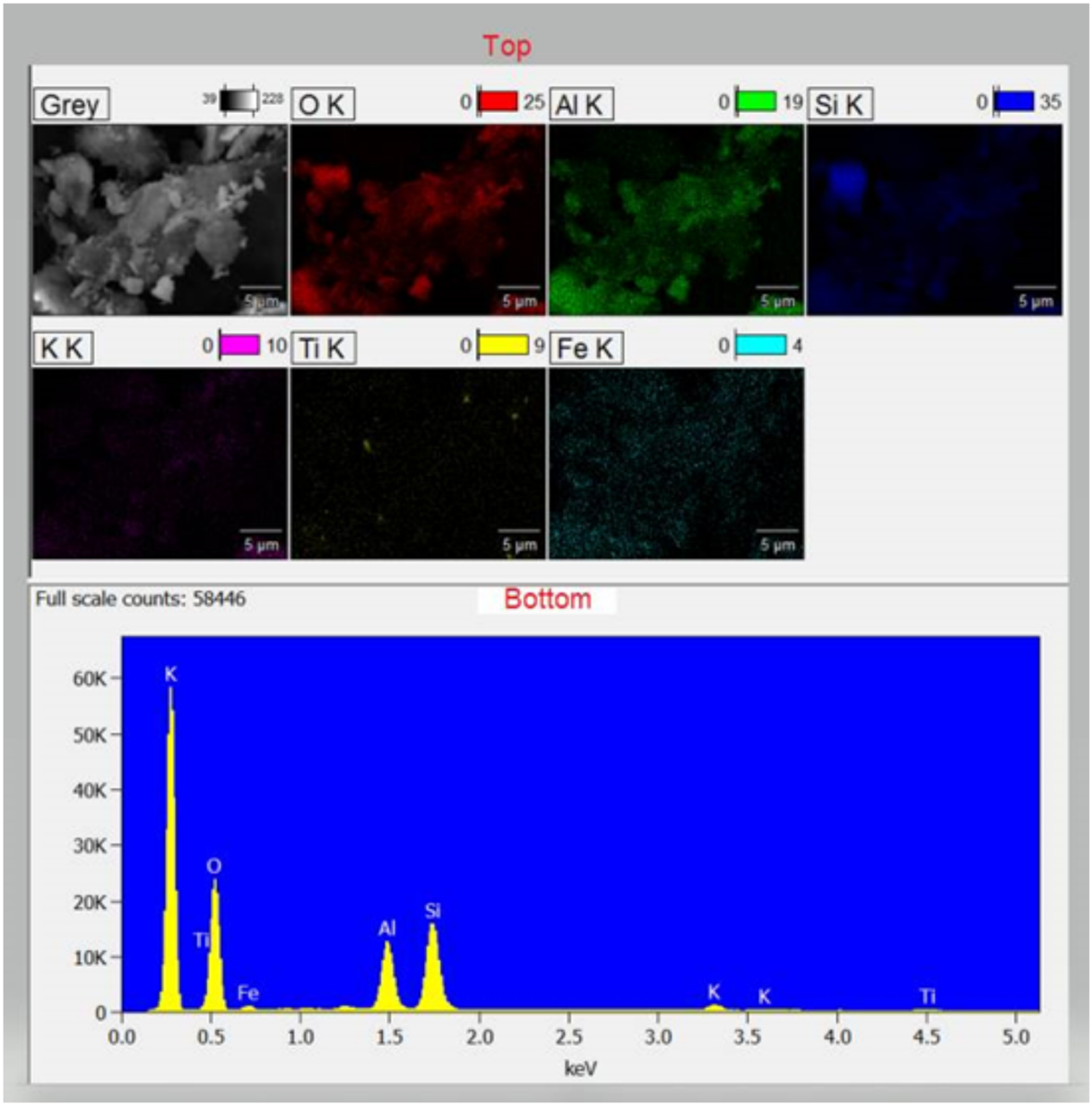

Fig. 2 (Top) Elemental mapping distribution of 10% CNT–GOL clay sample; (bottom) energy-dispersive X-ray spectroscopy spectrum of 10% CNT–GOL clay

peak 68°. SiO_2 and Al_2O_3 are the main components of these samples, and this is confirmed by bulk structures available bearing these phases including aluminium oxide silicate. Masheane et al. (2018) confirmed silica and alumina as the major constituents of the clay. Peaks identified at 2 θ of 24.28°, 42.70°, 50.38°, 64.29° and 81.42° are assigned to hematite phases. Furthermore, other elements (including calcium and potassium) identified by EDS and XRF are in the forms of diopside and potassian minerals of the clay. The XRF, XRD and EDS results revealed that the clay contains mainly SiO_2, Al_2O_3, Fe_2O_3 and TiO_2 which was successfully used as photocatalyst for the degradation of the methabenzthiazuron herbicide in water (Khennaoui et al. 2020).

The Fourier transform infrared spectroscopy (FTIR) spectra of GOL clay, 5% CNT–GOL clay and 10 % CNT–GOL clay samples are shown in Fig. 3b. The spectra show two peaks at 3698 cm^{-1} and 3618 cm^{-1}

Table 1 Mass percentage of chemical elements in GOL

Component	Mass %
SiO_2	64.04
Al_2O_3	23.02
Fe_2O_3	5.98
K_2O	2.37
TiO_2	2.34
MgO	0.87
CaO	0.36
P_2O_5	0.23

band due to stretching vibration hydroxyls. Minor bands at 3443 cm^{-1} for GOL clay blended with CNT were due to internal hydroxyls linked to the aluminium (Chargui et al. 2018). The absorption band presented at 1630 cm^{-1} can be attributed to the binding vibration of water molecules (which can be found between 1600 and 1650 cm^{-1}) (Boukhemkhem and Rida 2017; Hadjltaief et al. 2019) and or deformation of hydroxyl groups (O–H) (Leow et al. 2016). The sharper peak between 990 and 1035 cm^{-1} for the samples corresponds to silicon-oxygen bonds present in the clays (Terzopoulou et al. 2016; da Silva Lopes et al. 2019). The peak around 763 cm^{-1} is believed to be due to Ti-O-Ti bonds, while the absorption of Ti-O-Si is found around 926 cm^{-1} (Zeitler and Brown 1957). The presence of the band at 910 cm^{-1} is assigned to the Al–OH units linked to bulk structures of the clay samples (Boukhemkhem and Rida 2017; Chargui et al. 2018) and to the OH bending for clay admixed with CNT (Terzopoulou et al. 2016). The bands at 682 and 559 cm^{-1} correspond to the vibrations of Si–O–Al groups (Boukhemkhem and Rida 2017; da Silva Lopes et al. 2019). The functional groups identified agree with the chemical elements present as shown by elemental mapping and EDS spectrum in Fig. 2.

Optical analysis of GOL, 5% CNT–GOL and 10% CNT–GOL

The raw clay and clay with CNT were analysed for their photoresponse ability in order to confirm suitability as photocatalysts. The optical technique measurements were undertaken on GOL clay, 5% CNT–GOL, 10% CNT–GOL and on CNT (Fig. 4). Figure 4 b, c and d shows Kubelka–Munk function plots that were derived from the DRS (Fig. 2a) as previously reported (Muleja and Mamba 2018). The diffuse reflectance UV–vis spectrum (DRS) of the CNT reveals a shift in the far and near ultraviolet between 200 and 300 nm, respectively, and no other absorption was observed thereafter which agrees with previous work (Cheng et al. 2011). However, Khennaoui et al. (2020) have reported that Algerian natural clay showed an intense UV-vis absorption band situated at 201 nm and four weak bands situated at 243, 248, 366 and 430 nm. It was thought that balance between SiO_2 and TiO_2 could alter the photocatalytic activity of the mechanical mixed clay in this study. The investigation of these materials (GOL clay, 5% CNT–GOL, 10% CNT–GOL) showed reflectance on the violet light, for example, at 320 nm and another reflectance in the blue light ranging from 450 to 495 nm. This provided circumstantial evidence of the photocatalytic activity in both the UV and the visible lights, suggesting solar radiation may function as a suitable energy source. Two bands edge were observed for the GOL clay, 5% CNT–GOL and 10% CNT–GOL. The two absorption edges emanate from bulk structures and different phases of minerals revealed by XRF and XRD in Table 1 and Fig. 3a, respectively. For example, TiO_2 is known to possess two phases, namely, rutile and anatase which are responsible for two absorption edges in the composite sample (Nazarkovsky et al. 2014). Figure 4a implies that the materials combine the features of GOL clay (SiO_2, Al_2O_3, TiO_2, Fe_2O_3) and CNT resulting into new properties which could modify the process of the e^- / h^+ pair formation (Saleh and Gupta 2012). It is suggested that CNT improves the function and formation of the e^- / h^+ pair improving performance and stability of these materials for solar photodegradation of dyes in aqueous solutions.

The energy band for these materials was measured from the Kubelka–Munk function and the Tauc's relation of a curve $(F(R)hv)^2$ vs hv, where hv is the photon energy and $F(R)$ the reflectance factor that was transformed according to the Kubelka–Munk model from the reflectance R. The results (Fig. 4 a, b and c) show two energy band values for each material most likely due to different phases which characterize both pure GOL clay and mixed CNT–GOL samples. For GOL sample, the energy band gaps values are 2.75 eV and 3.25 eV within the range of previously reported values (Horwath and Liang 2011). Horwath and Liang (2011) reported that the energy band gap values of clays range from 1.5 to 6.5 eV. They also observed that the band gap energies vary depending on the chemical composition and overall atom % of the clay. In this study, the energy band gaps values are 1.75 and 3.24 eV and 1.53 and 2.90 eV

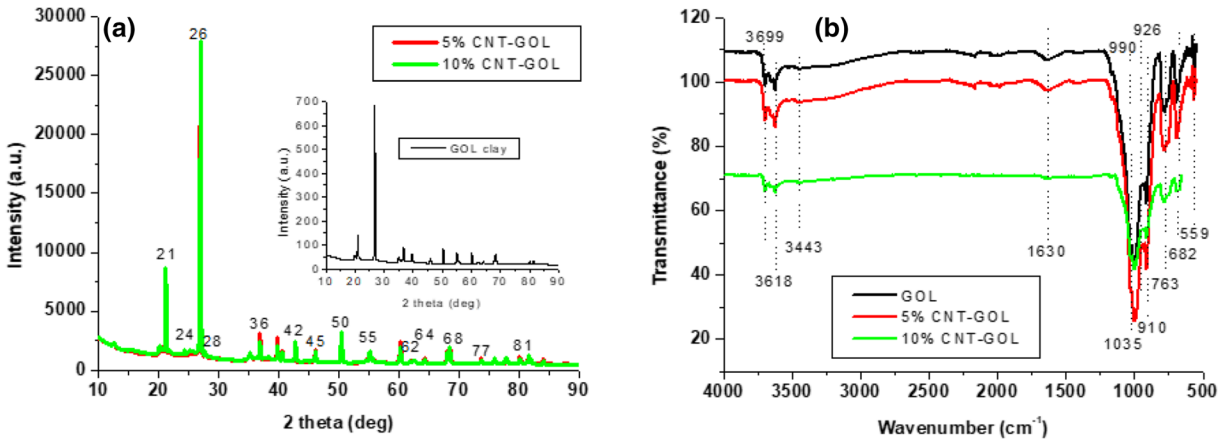

Fig. 3 **a** XRD patterns and chemical phase peaks and **b** FTIR spectra of GOL clay; 5% CNT–GOL and 10 % CNT–GOL samples

for 5% CNT–GOL and 10% CNT–GOL, respectively. The lowering of the energy band gap for these materials without considering the effect of CNT could be due to the presence of hematite whose energy band gap is reported to be 1.9–2.3 eV (Matsumoto 1996; Guo 2007). Furthermore, the energy band gap of TiO_2 is generally accepted to be 3.20 eV (Djouadi et al. 2018), hence contributing to the values obtained for the present materials. However, the decrease of the energy band gap for the CNT–GOL clay samples was attributed to CNT. This is because of the diversity in energy band gap in CNT which ranged from zero (metal-like) to as high as that of silicon because of the difference in the size and the structure (Collins and Avouris 2000; Wei et al. 2013). Wei et al. (2013) have reported even smaller values of the energy band gap (0.97, 1.09, and 1.02 eV) for pure and treated carbon nanotubes. The evidence shows that the introduction of CNT in the GOL clay has decreased the energy band gap from 3.25 to 1.53 eV. Hence, it is confirmed that the interaction between CNT and GOL clay would enhance the photocatalytic properties through formation of heterojunction.

Photocatalytic activity

Removal of BB dyes: effect of irradiation time and addition of H_2O_2

The removal of BB dyes from aqueous solution through photocatalytic degradation was measured with UV-vis spectroscopy. Figure 5 a shows that the removal of BB dyes increased for all three materials and decreased after 45 min of irradiation time. The results reveal that the removal of BB dyes improved gradually with the addition of 5% CNT and 10% CNT to GOL clay with the highest percentage achieved with 10% CNT addition. The positive link between BB removal and CNT addition indicated that CNT addition plays an important role stabilizing this oxidation process. At 45 min of irradiation time, the percentage of degradation was 65.76%, 79.44% and 94.71% for GOL clay; 5% CNT–GOL and 10% CNT–GOL, respectively. In this study, clay nanocomposites have demonstrated photoresponse as illustrated in Figs. 4 and 5. The removal of BB dyes could be attributed to the ability of clay and CNT to adsorb dyes on the photocatalysts. Both clay and CNT can behave as semiconductors. It is thought that the BB dyes are transferred through diffusion onto the semiconductors. The adsorption of BB dyes to the photocatalysts surface and excitation of the photocatalysts generates oxidizing radicals which unselectively degrade the macromolecule dyes. CNT acts as an efficient adsorption trap of the dye leading to rapid photocatalytic degradation (Saleh and Gupta 2012). Although adsorption is basic in photocatalysis, the current investigation emphasizes on the photocatalytic features of the combined clay and CNT samples.

Further experiments were carried out in a similar way but the only difference being the addition of hydrogen peroxide (H_2O_2) to the mixed slurry of photocatalysts containing the BB dye aqueous solution, and the results are displayed in Fig. 5 b, c and d. When 2 mmol, 4 mmol and 6 mmol of H_2O_2 were added to the suspensions, the photocatalytic activity of 10% CNT–GOL increased up to 100% degradation of BB dye in 15 min. At the same time the photodegradation of BB with GOL clay and 5% CNT–GOL clay was 61.77% and 69.75% for 2 mmol

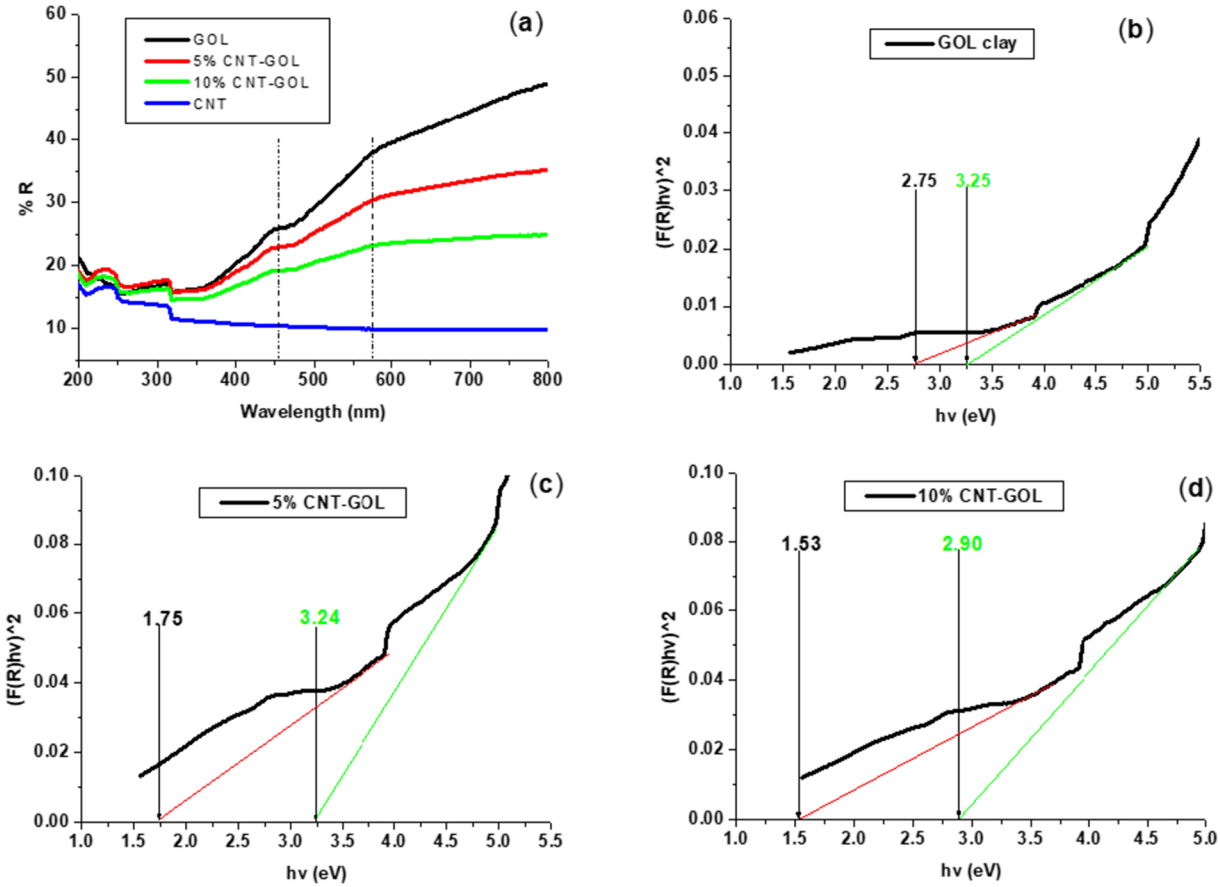

Fig. 4 (**a**) DRS of CNT, GOL clay, 5% CNT–GOL and 10% CNT–GOL showing absorptions above 380 nm and the Kubelka-Munk plots for (**b**) GOL clay, (**c**) 5% CNT–GOL and (**d**) 10% CNT–GOL depicting the energy band gaps values

(H_2O_2), 60.85% and 67.08% (4 mmol (H_2O_2), and 60.07% and 72.90% for 6 mmol (H_2O_2), respectively. Overall, these findings indicate that the amount of CNT added to the GOL clay is as much important as H_2O_2 to a certain extend. Ten percent CNT–GOL clay had the highest photocatalytic activity, reaching 86.68% and 100% degradation of BB dyes in 15 min without H_2O_2 and with H_2O_2, respectively (Fig. 5a, b). On the other hand, 62.49% and 86.68% of dyes were removed with GOL clay and 10% CNT–GOL clay, respectively, within the same irradiation time. The photodegradation was 24.19% higher when CNT was added to the clay without the addition of H_2O_2 and 13.32% with H_2O_2. Improved BB dyes photodegradation was achieved with the combination GOL and CNT, addition of an additional source of radicals led to reduced degradation rates, possibly due to radical scavenging.

These data show that when 10% of CNT is added to the natural GOL clay, 94.71% of BB dye pollutants are removed from the aqueous solution. The results also show that only small amount of H_2O_2 is enough to reach the highest value 100% of BB dye removed within 15 min. Therefore, the findings imply (i) using the GOL clay acts as an interface and provider of semiconductors (structural phases (XRD) and chemical compositions (XRF)); (ii) mixing with CNT (an electron giver and acceptor) coupled with 2 mmol of H_2O_2 (producer of oxidizing species (hydroxyl and superoxide radicals)) could have contributed to the photoresponse of the utilised materials as confirmed by DRS results. Other characterization techniques including FESEM, Maps-EDS and FTIR used revealed functional groups linked to titania, silica, alumina and hematite and a good distribution of each chemical element associated thereto in samples confirming their presence and possibility to react during the photocatalysis of BB dye. More details about possible phenomena interactions that are susceptible to occur are entailed in the mechanism section of this paper.

Figures 6 a to d show the photocatalytic activity of the raw and admixtures materials on the concentrations decay

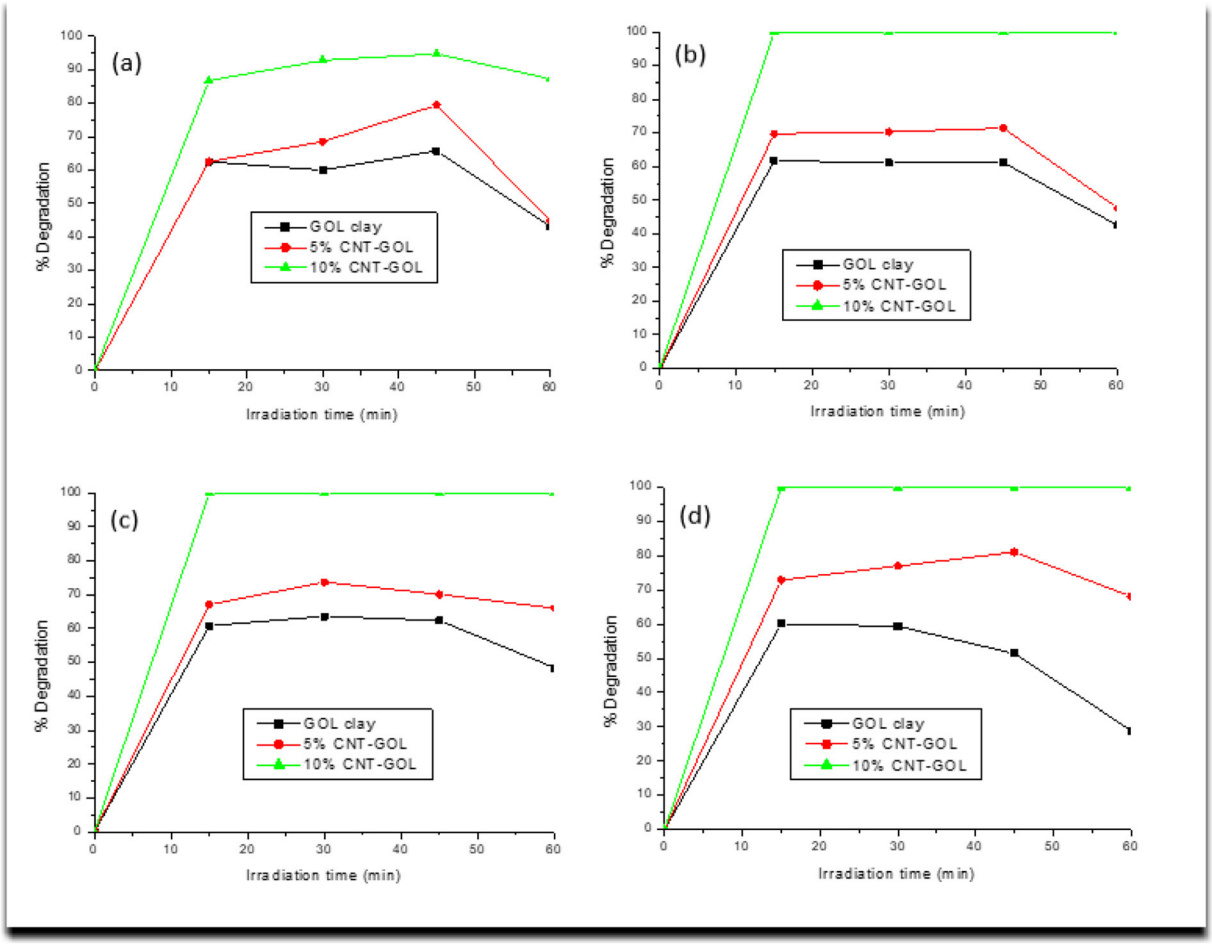

Fig. 5 **a** Photocatalytic activity of GOL clay, 5% CNT–GOL and 10% CNT–GOL in the degradation of BB dyes under visible light irradiation; for **b** 2 mmol; **c** 4 mmol and **d** 6 mmol of H_2O_2 was added, respectively

of BB dye as a function of irradiation time. The results confirm the trends observed in Figs. 4 and 5. The data indicate the disappearance of BB dye with irradiation time until 45 min for Fig. 6a whereas for Fig. 6b, c and d, different tendencies are obtained. The results obtained with 10% CNT–GOL suggest that there is an improvement in the performance which can be attributed to the synergy of the various components. These include structural chemical composition of GOL clay, CNT and the addition of H_2O_2. Photocatalytic reaction accounts for the electronic structure of the photocatalyst, and there are two critical factors that influence photocatalysis, namely, light absorption by the material and migration of light-induced electron holes (Asif et al. 2015). The combination might contribute to the collective features of a good photoresponse from the photocatalysts based on the ability to generating oxidising species such as hydroxyl and superoxide radicals, charge separation and transportation.

Photodegradation could be detailed as a combination of improved adsorption of dye molecules onto the catalyst surface, charge separation and transportation, visible light absorption and generation of sufficient amounts of the oxidizing species of the photocatalyst (Mamba et al. 2014). The data presented in Figs, 5 and 6 can be grouped in three scenarios: (i) Some of the dyes adsorbed during the initial step of the experiment (60-min run in the dark: not shown) might have not been completely decomposed with clay and clay mixed with 5% CNT. The absorbed light might not have been enough due to the small amount of CNT in the nanocomposite. So, some of the adsorbed dye molecules might have been released (after 45 min) into the solution during the photocatalytic experiment. To mitigate such shortfall, more time and or enough CNT might be required to facilitate

generation of enough oxidizing species and the charge separation and transportation for complete decay of the dyes. (ii) When hydrogen peroxide was added to the mixture particularly for 10% GOL–Clay, enough reactive oxidizing species were formed in the aqueous solution resulting in the complete decomposition of dyes. In this case, the adsorbed dyes during the 60-min dark experiment including enough light absorbed during the light experiment could have enhanced the synergy of GOL–CNT mixture prompting total discoloration in 15 min. Ten percent CNT–GOL reveals most of the features of reported good photocatalysts (Saleh and Gupta 2012) which could explain the fast initial (15 min) decrease of dye concentration observed. The recombination kinetics of charge carriers might have been reduced and/or eliminated by the synergy of clay composition and CNT hence the improved removal of BB dyes obtained. Photocatalytic results could imply that both the aromatic rings and the azo groups of BB dyes are cleaved during photocatalytic reactions (Abidin et al. 2015). (iii) Further observation of the data available in Fig. 6 from time 0 to 60 min under irradiation, it seems that the constant of the kinetic equation might not very identifiable, mainly in the case of 10% CNT–GOL. The first measurement at 15 min already has all the concentration removed. It means that any rate higher that certain value would be also totally able to explain the experimental data. In addition, the increase in Ct/Ci for time 60 min cannot be explained by the commonly used models, namely, Langmuir–Hinshelwood (Kumar et al. 2008; Asif et al. 2015) and the pseudo-zero, pseudo-first and pseudo-second-order kinetic models (Gaya., 2013). For future purpose, more experimental points would be needed before 15 min to have enough data to make the model easily identifiable. This is because 10% CNT–GOL demonstrated high efficiency within a short period of time than expected. The photocatalytic behaviour of 10% CNT–GOL nanocomposite would be better investigated with shorter time (i.e. every 5 min instead of 15 min) interval for taking aliquots. As such, we thought outside classical procedure to measure kinetics studies. The kinetic information obtained with these data is then carefully explained by only considering the first 45 min of the experiments. Data depicted in Figs. 5 and 6a obtained without the addition of H_2O_2 during the 45 min of the photocatalytic experiments were considered for the kinetic studies.

The Langmuir–Hinshelwood model was used, in the simplified form represented by Eq. (2), to describe the kinetics of photocatalytic reactions of small concentration in aqueous solutions:

$$\ln\frac{C_i}{C_f} = k_{app}t \tag{2}$$

where Ci is the initial concentration (ppm or mg L^{-1}) of BB dye after adsorption and Ct is the concentration (ppm or mg L^{-1}) of BB dye at time t during photocatalytic process. K_{app} stands for the pseudo-first-order reaction rate constant (min^{-1}), and t is irradiation time (min) during the photocatalytic reaction. The results are presented in Fig. 7 for GOL clay, 5% CNT–GOL and 10% CNT–GOL photocatalysts. It is obvious from the linear fitting that the obtained data do not satisfactorily obey the pseudo-first-order kinetic model (Fig. 7 (left hand side)).

Most dye-based oxidation studies rely on the disappearance of the initial concentration of dyes (Gaya 2013). As such, the photocatalytic activity of the catalysts can be quantitatively evaluated by second-order kinetic model in Eq. (3) where Ci and Ct are the initial concentration and concentration of BB dye at time (t) during the photocatalytic reaction, respectively.

$$-\frac{1}{[C_t]} + \frac{1}{[C_i]} = -kt \tag{3}$$

A satisfactory fit was obtained for the photocatalysts that contain CNT (5% CNT–GOL and 10% CNT–GOL) in their composition as shown (Fig. 7 (right hand side)) in agreement with previous reports (Kumar et al. 2008; Wang et al. 2015).

The photocatalytic experiments obtained in this study (at least for the points considered up to 45 min) show that the data fit well second-order kinetic. This is important because it has been reported that an assumed reaction network leads to a single kinetic model, but a common model, the Langmuir–Hinshelwood rate equation, arises from multiple mechanisms; hence, models alone do not reveal unique mechanisms (Ollis 2018). And the findings described herewith might worth sharing to inform researchers that certain photocatalytic

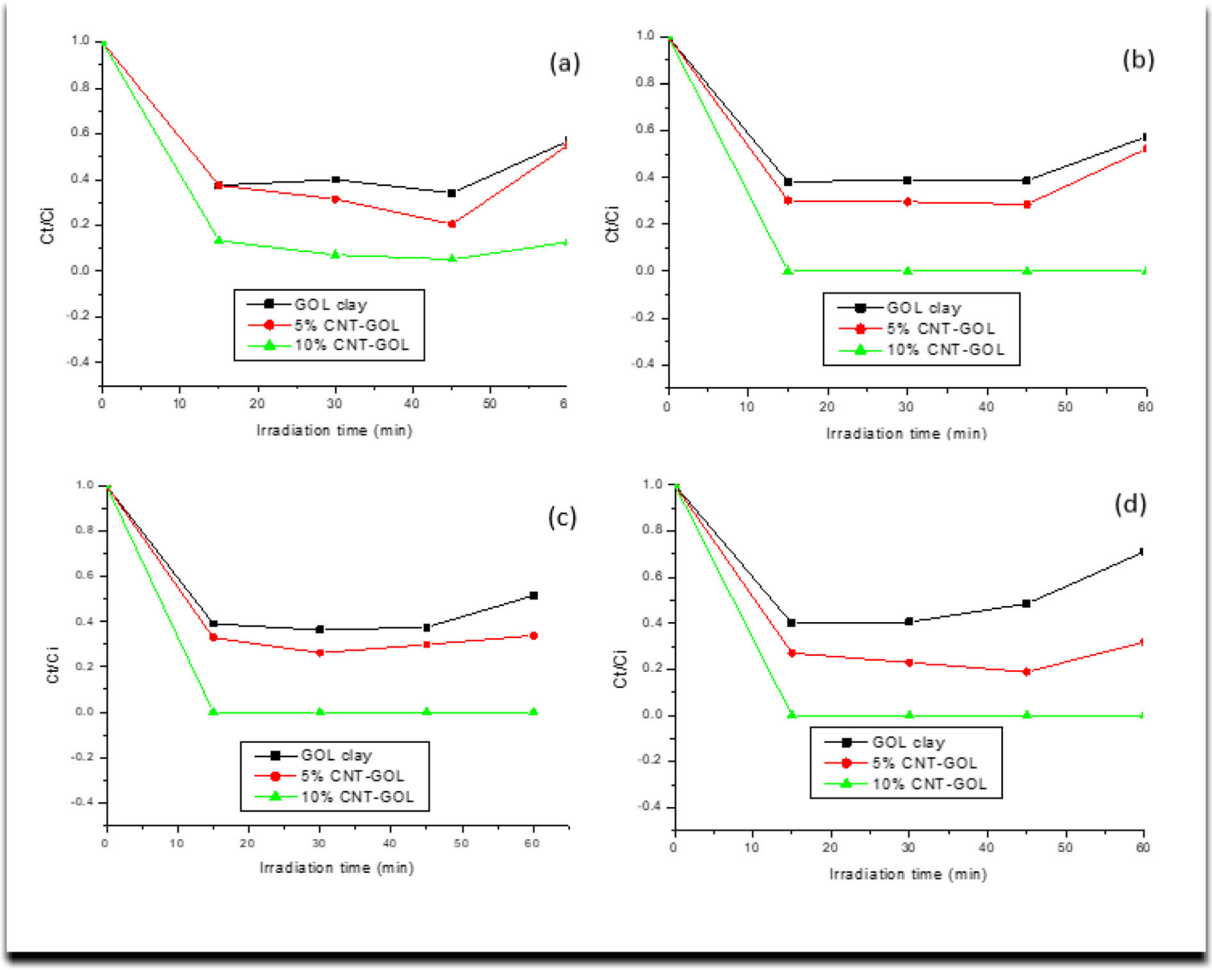

Fig. 6 **a** Mineralization of BB dyes using GOL clay, 5% CNT–GOL and 10% CNT–GOL as photocatalysts under the visible light irradiation time; and for (**b**) 2 mmol, (**c**) 4 mmol and (**d**) 6 mmol of H_2O_2 was added, respectively

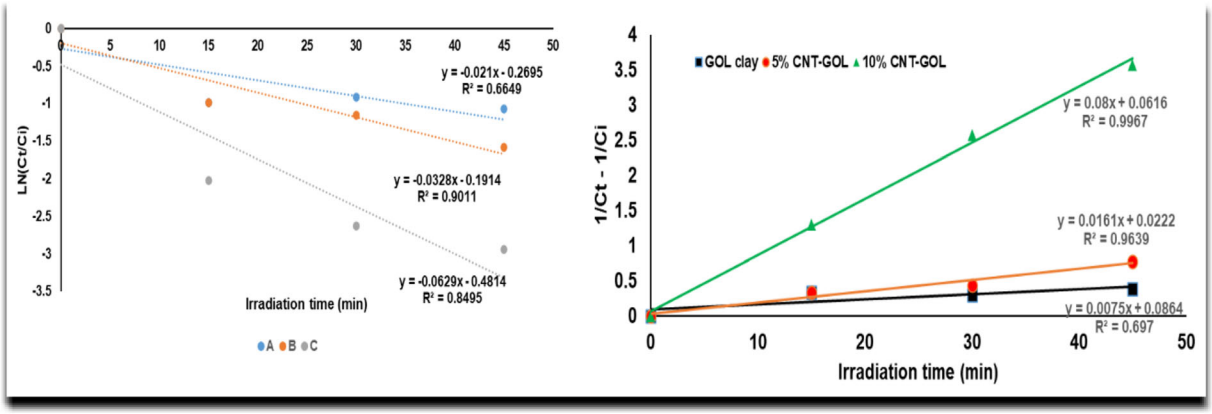

Fig. 7 (Left hand side) Pseudo-first-order kinetics of BB dyes degradation using GOL clay (A), 5% CNT–GOL (B) and 10% CNT–GOL (C) as photocatalysts under 45 min of visible light irradiation and (right hand side) second-order model kinetics of BB dyes degradation using GOL clay, 5% CNT–GOL and 10% CNT–GOL as photocatalysts under 45 min of visible light irradiation

experimental data might deviate from the classical procedure; alternative thinking might be necessary.

Proposed photocatalytic mechanism

The presence of CNT plays a role of semiconductor (Collins and Avouris 2000) which emphasized the good quality of the 10% CNT–GOL sample to operate as a photocatalyst. The photodegradation of BB dyes was then improved by the ability of CNT to behave as an electron donor and acceptor. This is very crucial because, during photocatalysis, the excited e− in the conduction band of clay (SiO_2, Al_2O_3, TiO_2, Fe_2O_3) migrates into CNT, of which have a special structure and the ability for e− transport. Even interesting is that GOL clay acts as photoactive material and catalyst for the photodegradation (Martínez-Costa et al. 2018). Thus, the possibility of the e^- / h^+ pairs recombination decreases. Meanwhile, the adsorbed oxygen (O_2) on the surface of CNTs may accept e^- and form radicals ($^{\bullet}O_2^-$), which also leads to the formation of other oxidizing species ($^{\bullet}OH$) in the system. Therefore, there are more radicals in the system, resulting in the quicker degradation of the BB dyes (Yu et al. 2005; Saleh and Gupta 2012). In this paper, the effect of H_2O_2 while varying the molar concentration to the aqueous solution of BB dyes during the photocatalytic experiments was assessed. H_2O_2 is one of the most used radical scavengers in photocatalysis (Muleja and Mamba 2018). This is because H_2O_2 is a stronger electron acceptor than oxygen that can react with an electron emitted from the valence band of the photocatalyst to generate $^{\bullet}OH$ and OH^- (Chu et al. 2007). Additionally, photoexcitation reaction of H_2O_2 produces $^{\bullet}OH$ species (Xu et al. 2019) as displayed in Eq. (7), while Eq. (8) shows that more $^{\bullet}OH$ can be produced in the presence of $^{\bullet}O_2^-$. The results from H_2O_2 experiments confirm the important role of h^+ and $^{\bullet}OH$ during photocatalysis. The mixing of CNT and GOL clay could create an interface that can reduce the recombination of charge carrier pairs by the way of effective charge migration and separation, leading to the enhanced photocatalytic activity. Other researchers observed similar scenarios with different materials (Yin et al. 2016; Luo et al. 2019). The basic mechanism for the photodegradation of BB dyes with 10% CNT–GOL (CNT-Clay) is represented by the Eqs. (4), (5), (6), (7), (8), (9), (10) to (11).

$$C_2O_2 \xrightarrow{hv} 2HO^{\bullet} \tag{4}$$

$$H_2O_2 + O_2^{\bullet-} \rightarrow HO^{\bullet} + O_2 + OH^- \tag{5}$$

$$\text{CNT}-\text{Clay} + hv \rightarrow \text{CNT}-\text{Clay}\left(e_{CB}^- + hv_{VB}^+\right) \tag{6}$$

$$\text{CNT}-\text{Clay}\left(h_{VB}^+\right) + H_2O \rightarrow \text{CNT}-\text{Clay} + HO^{\bullet} + H^+ \tag{7}$$

$$\text{CNT}-\text{Clay}\left(h_{VB}^+\right) + HO^- \rightarrow \text{CNT}-\text{Clay} + HO^{\bullet} \tag{8}$$

$$\text{CNT}-\text{Clay}\left(e_{CB}^-\right) + O_2 \rightarrow \text{CNT}-\text{Clay} + O_2^{\bullet-} \tag{9}$$

$$\text{CNT}-\text{Clay}\left(e_{CB}^-\right) + O_2^{\bullet-} \rightarrow \text{CNT}-\text{Clay} + H_2O_2 \tag{10}$$

$$\text{BB} + OH^- + O_2^{\bullet-} + h^+ \rightarrow CO_2 + H_2O + \text{Organic compounds} + \text{Inorganic acids} \tag{11}$$

Based on the above explanation, a mechanism of the mineralization of BB dyes under visible light irradiation is therefore suggested in a schematic representation in Fig. 8.

Total organic content analysis

Total organic content (TOC) analysis was used to investigate the amount of carbon element in organic compounds left in the aqueous solution after the photocatalytic experiments. This is important because it determines the level of BB dyes degradation during the photocatalysis with GOL clay, 5% CNT–GOL and 10% CNT–GOL materials. The TOC values of BB dye molecules removal were compared with the photodegradation removal percentage in order to estimate the level of mineralization of BB dyes. The results from the experiments carried out within 60 min are summarized in Table 2.

From Table 2, when GOL and 5% CNT–GOL are used, less than half (35.97% and 39.95%) of the amount of BB dyes molecules were removed. Yet with 10% CNT–GOL, higher removal percentage (87.22%) was obtained for the degradation of BB dyes. The data confirm

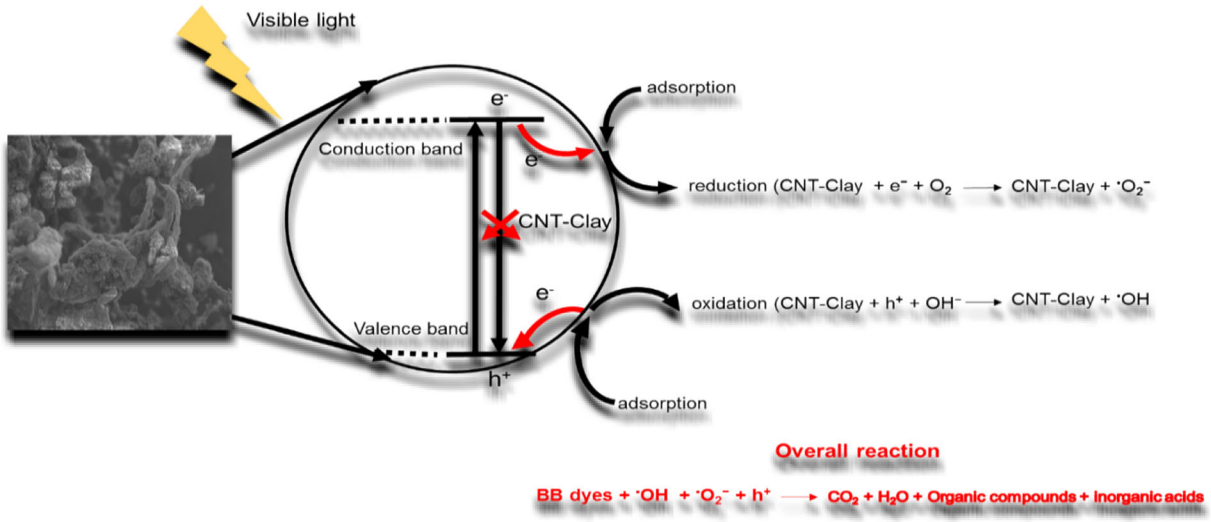

Fig. 8 Proposed mechanism of photocatalytic degradation of BB dyes using 10% CNT–GOL catalyst

that when 10% CNT–GOL photocatalyst is used, a higher degree of complete mineralization of the dye molecules, which is desirable, was achieved. Higher TOC removal values indicate that the dye molecules are broken down into smaller colourless products first before being mineralized to carbon dioxide, water and other inorganic species (Mamba et al. 2014). The results also show that a certain amount of organic degradation by-products remain in solution. The current mineralization percentage of BB dye molecules is higher (87%) than previously reported 61% (Nzaba et al. 2018) and 62% (Mukonza et al. 2017) within an hour of visible light irradiation implying that GOL–CNT could be more suitable for the removal of BB dyes from aqueous solution.

Table 2 also reveals that when CNT was added to the natural clay, the percentage of BB dye molecule removal increased for both TOC and degradation from 35.97 to 86.14% and 43.02 to 87.22% for GOL and 10% CNT–GOL, respectively. The findings are interesting because they entail that CNT contributes significantly to the degradation of BB dyes in aqueous solution. There is a close correlation between the two values. However, when natural clay is used, the level of TOC removal and that of degradation are 7.05% apart indicating that some of the removal is due to the adsorption process which was expected because adsorption is desired for photocatalysis. The same observation is evident with 5% CNT–GOL where 4.91% less removal was obtained. On overall photocatalytic activity on BB dyes, a comparative survey shows that 10% CNT–GOL performed better within an hour than PAMAM templated N, Pt co-doped TiO_2 (Nzaba et al. 2018) and F, Sm^{3+} co-doped TiO_2 (Mukonza et al. 2017). Another advantage of the 10% CNT–GOL photocatalyst is that at the end of experiments, the sedimentation and decantation of materials was easy and fast (Chen et al. 2004) which would be essential for future study on recycling.

Table 2 Removal values for the degradation of BB dyes and TOC analysis of BB dyes in aqueous solution at time 60 min of solar light irradiation

Percentage removal	GOL clay	5% CNT–GOL	10% CNT–GOL
TOC	35.97	39.95	86.14
Degradation	43.02	44.86	87.22

Conclusion

In this paper, natural clay and carbon nanotubes were mechanically mixed. The mixing produced natural nanocomposites with enhanced photocatalytic activity. Natural clay contains 2.34% of TiO_2 which is crucial in photocatalysis, and the DRS revealed that the materials can be used as photocatalysts. The addition of CNT to GOL reduced the energy band gaps from 3.25 (GOL) to 2.90 eV (10% CNT–GOL) and 2.75 eV (GOL) to 1.53 eV (10% CNT–GOL) for the first and second absorption bands, respectively. CNT contributed to the enhancement of the photocatalytic activity of CNT–GOL nanocomposites through the charges migration, separation and

reduction of the recombination of the e^- / h^+ pairs. Furthermore, the mixing of CNT and GOL created a synergy and formation of a heterojunction like interface improving the photocatalytic features of the nanocomposites. All these aspects added to the production of highly oxidizing radical species which attacked the azo and amines groups in BB dyes leading to their degradation. The kinetic data (based on 45 min time of light irradiation) showed that the photocatalysis decay of BB dyes fit well the second-order model. The TOC results showed that 87% of the BB dye molecules were completely mineralized in 60 min when 10% CNT–GOL was used. The 10% CNT–GOL successfully removed 95% BB dyes, while 66% removal was obtained for the GOL. The performance was further increased with the addition of 2 mmoL of H_2O_2 within 15 min of solar light irradiation. The current study showed that when optimized natural clay mixed with CNT could find application as a modified photocatalytic filter for the treatment of wastewaters in the rural areas where clays and sun light are readily available.

Funding This work was financially supported by the University of South Africa (UNISA) at the Institute for Nanotechnology and Water Sustainability (iNanoWS), College of Science, Engineering and Technology (CSET).

Declarations

Conflict of interest The authors declare that there is no conflict of interest.

References

Abidin CZA, Fahmi MR, Soon-An O, Makhtar SNNM, Rahmat NR (2015) Decolourization of an azo dye in aqueous solution by ozonation in a semi-batch bubble column reactor. Sci Asia 41:49–54

Al-Kdasi A, Idris A, Saed K, Guan CT (2004) Treatment of textile wastewater by advanced oxidation processes—a review. Global Nest: the Int J 6(3):222–230

Asif SAB, Khan SB, Asiri AM (2015) Visible light functioning photocatalyst based on Al2O3 doped Mn3O4 nanomaterial for the degradation of organic toxin. Nanoscale Res Lett 10(1):355

Boukhemkhem A, Rida K (2017) Improvement adsorption capacity of methylene blue onto modified Tamazert kaolin. Adsorpt Sci Technol 35(9-10):753–773

Brüschweiler BJ, Merlot C (2017) Azo dyes in clothing textiles can be cleaved into a series of mutagenic aromatic amines which are not regulated yet. Regul Toxicol Pharmacol 88:214–226

Chargui F, Hamidouche M, Belhouchet H, Jorand Y, Doufnoune R, Fantozzi G (2018) Mullite fabrication from natural kaolin and aluminium slag. Boletín de la Sociedad Española de Cerámica y Vidrio 57(4):169–177

Chen Y, Wang K, Lou L (2004) Photodegradation of dye pollutants on silica gel supported TiO2 particles under visible light irradiation. J Photochem Photobiol A Chem 163(1-2):281–287

Cheng X, Zhong J, Meng J, Yang M, Jia F, Xu Z, Kong H, Xu H (2011) Characterization of multiwalled carbon nanotubes dispersing in water and association with biological effects. J Nanomater 2011:14

Chu W, Choy WK, So TY (2007) The effect of solution pH and peroxide in the TiO2-induced photocatalysis of chlorinated aniline. J Hazard Mater 141(1):86–91

Collins PG, Avouris P (2000) Nanotubes for electronics. Sci Am 283(6):62–69

da Silva Lopes J, Rodrigues WV, Oliveira VV, Braga ADNS, da Silva RT, França AAC, da Paz EC, Osajima JA, da Silva Filho EC (2019) Modification of kaolinite from Pará/Brazil region applied in the anionic dye photocatalytic discoloration. Appl Clay Sci 168:295–303

Djouadi L, Khalaf H, Boukhatem H, Boutoumi H, Kezzime A, Santaballa JA, Canle M (2018) Degradation of aqueous ketoprofen by heterogeneous photocatalysis using Bi2S3/TiO2–Montmorillonite nanocomposites under simulated solar irradiation. Appl Clay Sci 166:27–37

Ebbesen TW, Lezec HJ, Hiura H, Bennett JW, Ghaemi HF, Thio T (1996) Electrical conductivity of individual carbon nanotubes. Nature. 382:54–56

Gaya UI 2013 Heterogeneous photocatalysis using inorganic semiconductor solids. Springer Science and Business Media

Gournis D, Karakassides MA, Bakas T, Boukos N, Petridis D (2002) Catalytic synthesis of carbon nanotubes on clay minerals. Carbon 40(14):2641–2646

Guldi DM, Rahman GMA, Zerbetto F, Prato M (2005) Carbon nanotubes in electron donor−acceptor nanocomposites. Acc Chem Res 38(11):871–878

Guo, J. 2007 Electronic structure characterization and bandgap engineering of solar hydrogen materials. In Solar Hydrogen and Nanotechnology II (Vol. 6650, p. 66500F). International Society for Optics and Photonics.

Hadjltaief HB, Gálvez ME, Zina MB, Da Costa P (2019) TiO2/clay as a heterogeneous catalyst in photocatalytic/photochemical oxidation of anionic reactive blue 19. Arab J Chem 12(7):1454–1462

Hamza W, Dammak N, Hadjltaief HB, Eloussaief M, Benzina M (2018) Sono-assisted adsorption of cristal violet dye onto tunisian smectite clay: characterization, kinetics and adsorption isotherms. Ecotoxicol Environ Saf 163:365–371

Herrmann JM (1999) Heterogeneous photocatalysis: fundamentals and applications to the removal of various types of aqueous pollutants. Catal Today 53(1):115–129

Horwath W, and Liang YL (2011). Variations of Chemical Composition and Band Gap Energies in Hectorite and Montmorillonite Clay Minerals on Sub-Micron Length Scales. Final Report. Kearney Foundation of Soil Science.

Kausar A, Iqbal M, Javed A, Aftab K, Bhatti HN, Nouren S (2018) Dyes adsorption using clay and modified clay: a review. J Mol Liq 256:395–407

Khennaoui B, Zehani F, Malouki MA, Menacer R, López MC (2020) Chemical and physical characterization of a natural

clay and its use as photocatalyst for the degradation of the methabenzthiazuron herbicide in water. Optik 219:165024
Kumar KV, Porkodi K, Rocha F (2008) Langmuir–Hinshelwood kinetics–a theoretical study. Catal Commun 9(1):82–84
Leow WR, Ng WKH, Peng T, Liu X, Li B, Shi W, Lum Y, Wang X, Lang X, Li S, Mathews N (2016) Al2O3 surface complexation for photocatalytic organic transformations. J Am Chem Soc 139(1):269–276
Li J, Bishop PL (2002) In situ identification of azo dye inhibition effects on nitrifying biofilms using microelectrodes. Water Sci Technol 46(1-2):207–214
Luo J, Luo Y, Yao J, Zhang M, Chen S, Liu X (2019) Composite microsphere resulting from assembly of BiOCl nanosheets and palygorskite nanorods for enhanced photocatalytic activity. Appl Clay Sci 168:450–458
Mamba G, Mamo MA, Mbianda XY, Mishra AK (2014) Nd, N, S-TiO_2 decorated on reduced graphene oxide for a visible light active photocatalyst for dye degradation: Comparison to its MWCNT/Nd, N, S-TiO_2 analogue. Ind Eng Chem Res 53(37):14329–14338
Martínez-Costa JI, Rivera-Utrilla J, Leyva-Ramos R, Sánchez-Polo M, Velo-Gala I (2018) Individual and simultaneous degradation of antibiotics sulfamethoxazole and trimethoprim by UV and solar radiation in aqueous solution using bentonite and vermiculite as photocatalysts. Appl Clay Sci 160:217–225
Masheane M, Nthunya L, Mubiayi M, Thamae T, Mhlanga S (2018) Physico-chemical characteristics of some Lesotho's clays and their assessment for suitability in ceramics production. Part Sci Technol 36(1):117–122
Matsumoto Y (1996) Energy positions of oxide semiconductors and photocatalysis with iron complex oxides. J Solid State Chem 126(2):227–234
Molinari R, Lavorato C, Argurio P (2017) Recent progress of photocatalytic membrane reactors in water treatment and in synthesis of organic compounds. A review. Catal Today 281:144–164
Mukonza SS, Nxumalo EN, Mamba BB and Mishra AK (2017) Enhanced solar light photodegradation of brilliant black bisazo dye in aqueous solution by F,Sm^{3+} codoped TiO2. IOP Conference Series: Materials Science and Engineering (Vol. 195, No. 1, p. 012006). IOP Publishing.
Muleja AA, Mamba BB (2018) Development of calcined catalytic membrane for potential photodegradation of Congo red in aqueous solution. J Environ Chem Eng 6(4):4850–4863
Muleja AA, Mbianda XY, Krause RW, Pillay K (2012) Synthesis, characterization and thermal decomposition behaviour of triphenylphosphine-linked multiwalled carbon nanotubes. Carbon 50(8):2741–2751
Nazarkovsky MA, Gun'ko VM, Wójcik G, Czech B, Sobieszek A, Skubiszewska-Zięba J, Janusz W, Skwarek E (2014) Band-gap change and photocatalytic activity of silica/titania composites associated with incorporation of CuO and NiO. Chem PhysicsTechnol Surf 5:421–437
Nzaba SKM, Ntsendwana B, Mamba BB, Kuvarega AT (2018) PAMAM templated N, Pt co-doped TiO2 for visible light photodegradation of brilliant black. Environ Sci Pollut Res 25(15):15146–15158
Oh SW, Kang MN, Cho CW, Lee MW (1997) Detection of carcinogenic amines from dyestuffs or dyed substrates. Dyes Pigments 33(2):119–135
Oh WC, Zhang FJ, Chen ML (2010) Characterization and photodegradation characteristics of organic dye for Pt–titania combined multi-walled carbon nanotube composite catalysts. J Ind Eng Chem 16(2):321–326
Ollis DF (2018) Kinetics of photocatalyzed reactions: five lessons learned. Front Chem 6:378
Paredes SP, Valenzuela MA, Fetter G, Flores SO (2011) TiO_2/MgAl layered double hydroxides mechanical mixtures as efficient photocatalysts in phenol degradation. J Phys Chem Solids 72(8):914–919
Rafii F, Hall JD, Cerniglia CE (1997) Mutagenicity of azo dyes used in foods, drugs and cosmetics before and after reduction by Clostridium species from the human intestinal tract. Food Chem Toxicol 35(9):897–901
Saleh TA, Gupta VK (2012) Photo-catalyzed degradation of hazardous dye methyl orange by use of a composite catalyst consisting of multi-walled carbon nanotubes and titanium dioxide. J Colloid Interface Sci 371(1):101–106
Terzopoulou Z, Bikiaris DN, Triantafyllidis KS, Potsi G, Gournis D, Papageorgiou GZ, Rudolf P (2016) Mechanical, thermal and decomposition behavior of poly (ε-caprolactone) nanocomposites with clay-supported carbon nanotube hybrids. Thermochim Acta 642:67–80
Todorova N, Giannakopoulou T, Karapati S, Petridis D, Vaimakis T, Trapalis C (2014) Composite TiO_2/clays materials for photocatalytic NOx oxidation. Appl Surf Sci 319:113–120
Wang Y, Zhou A, Jiang Y, Chen X, He J (2015) Tetraamino-zinc phthalocyanine covalently bound to benzoic acid-functionalized graphene composites for highly efficient visible light photocatalytic activities. RSC Adv 5(47):37823–37829
Wei H, Gu H, Guo J, Wei S, Guo Z (2013) Multiwalled carbon nanotubes with tuned surface functionalities for electrochemical energy storage. ECS J Solid State Sci Technol 2(10): M3008–M3014
Xu M, Pan G, Meng Y, Guo Y, Wu T, Chen H (2019) Effect of Ce3+ on the photocatalytic activity of MAlCe ternary hydrotalcites-like compounds in methylene blue photodegradation. Appl Clay Sci 170:46–56
Yamaguchi K, Inumaru K, Oumi Y, Sano T, Yamanaka S (2009) Photocatalytic decomposition of 2-propanol in air by mechanical mixtures of TiO2 crystalline particles and silicalite adsorbent: the complete conversion of organic molecules strongly adsorbed within zeolitic channels. Microporous Mesoporous Mater 117(1-2):350–355
Yin S, Di J, Li M, Fan W, Xia J, Xu H, Sun Y, Li H (2016) Synthesis of multiwalled carbon nanotube modified BiOCl microspheres with enhanced visible-light response photoactivity. CLEAN–Soil, Air, Water 44(7):781–787
Yu Y, Jimmy CY, Chan CY, Che YK, Zhao JC, Ding L, Ge WK, Wong PK (2005) Enhancement of adsorption and photocatalytic activity of TiO2 by using carbon nanotubes for the treatment of azo dye. Appl Catal B Environ 61(1-2):1–11
Zeitler VA, Brown CA (1957) The infrared spectra of some Ti-O-Si, Ti-O-Ti and Si-O-Si compounds. J Phys Chem 61(9): 1174–1177
Zhu W, Miser DE, Chan WG, Hajaligol MR (2004) Characterization of combustion fullerene soot, C60, and mixed fullerene. Carbon 42(8-9):1463–1471